Depths of the 410-km and 660-km discontinuities in and around the stagnant slab beneath the Philippine Sea: Is water stored in the stagnant slab?

Daisuke Suetsugu [a,*], Toru Inoue [b], Masayuki Obayashi [a], Akira Yamada [b], Hajime Shiobara [c], Hiroko Sugioka [a], Aki Ito [a], Toshihiko Kanazawa [c], Hitoshi Kawakatsu [c], Azusa Shito [a], Yoshio Fukao [a]

[a] Institute for Research on Earth Evolution, Japan Agency for Marine-Earth Science and Technology, Yokosuka, Kanagawa 237-0061, Japan
[b] Geodynamics Research Center, Ehime University, Matsuyama 790-8577, Japan
[c] Earthquake Research Institute, University of Tokyo, 1-1-1 Yayoi, Bunkyo-ku, Tokyo 113-0032, Japan

ARTICLE INFO

ABSTRACT

We determined the depths of the 410-km and 660-km seismic discontinuities (called "410" and "660," respectively, hereafter) beneath the Philippine Sea and the northwestern Pacific by the receiver function method; we used the broadband data obtained from broadband ocean-bottom seismographs. We found a very deep "660" at 691 km in the stagnant slab beneath the Philippine Sea. In the surrounding Philippine Sea regions and northwestern Pacific, the "660" appears at depths of 659–674 km. Comparison of the "660" depth and P-velocity anomalies indicated that temperatures in the stagnant slab are lower than that in the mantle transition zone (MTZ) beneath the northwestern Pacific by about 500 K. The temperature in the MTZ beneath the Parece Vela Basin and West Philippine Sea Basin, which surrounds the stagnant slab, is lower than that in the MTZ beneath the Pacific by about 200 K. The water content in the stagnant slab ($\sim$0.2 wt% H_2O) is higher than that in the other regions; however, the large uncertainty in the estimated water content ($\pm$0.2–0.3 wt% H_2O) prevents us from arriving at a definitive conclusion regarding the presence of water in the stagnant slab. Therefore, it is desirable to use other geophysical parameters (e.g., electrical conductivity) along with the seismic parameters in order to obtain an accurate estimate of the water content in the MTZ.

© 2010 Elsevier B.V. All rights reserved.

1. Introduction

The presence or absence of the water in the mantle has great implications for the dynamics and evolution of the earth (e.g., Williams and Hemley, 2001; Rüpke et al., 2006), since the water decreases the viscosity (e.g., Dixson et al., 2004) and solidus temperature (e.g., Karato and Jung, 1998). There is increasing evidence for the transport of water into the upper mantle beneath subduction zones (e.g., Shito et al., 2006; Iwamori, 2007; Kawakatsu and Watada, 2007). The oceanic crust and sediment in a subducted slab in the upper mantle are dehydrated, and the released water reduces the solidus temperature of the materials in the overlying upper mantle. This results in magma production, which is responsible for arc volcanism (e.g., Tatsumi, 1989). However, the depth to which water can penetrate the mantle transition zone (MTZ) and the lower mantle has not yet been clarified. The MTZ, which lies between the 410-km and 660-km seismic discontinuities (called "410" and "660", respectively), can act as a large water reservoir (e.g., Smyth,

1987; Inoue et al., 1995; Kohlstedt et al., 1996). Wadsleyite and ringwoodite can store up to 2–3 wt% of water and hence have greater storage capacity than do olivine in the upper mantle and perovskite and magnesiowüstite in the lower mantle (e.g., Bolfan-Casanova et al., 2003; Ohtani et al., 2004; Mosenfelder et al., 2006; Inoue et al., this issue). Extensive studies have been performed to demonstrate the presence of water in the MTZ from seismic structure (e.g., Van der Meijde et al., 2003; Suetsugu et al., 2006; Meier et al., 2009; Yamada, 2009) and electrical conductivity structure (e.g., Ichiki et al., 2006, 2001; Huang et al., 2005; Yoshino et al., 2008; Dai and Karato, 2009; Kelbert et al., 2009). However, no conclusive results have been obtained thus far.

There are three possible routes for the transportation of water into the MTZ. (1) The subducted oceanic crust can transport water even after dehydration in the uppermost mantle. Recent experimental and simulation studies have indicated that the crust should be fully dehydrated before it reaches the MTZ (Iwamori, 2007). (2) Water may be transported from the "mantle" of a subducted slab (Rüpke et al., 2004), because of which deep earthquakes may occur (Omori et al., 2004). (3) The overlying upper mantle may be hydrated by the water released from a slab in the upper mantle. The water may be transported into the MTZ by the downgoing flow

* Corresponding author. Tel.: +81 468 67 9750; fax: +81 468 67 9315.
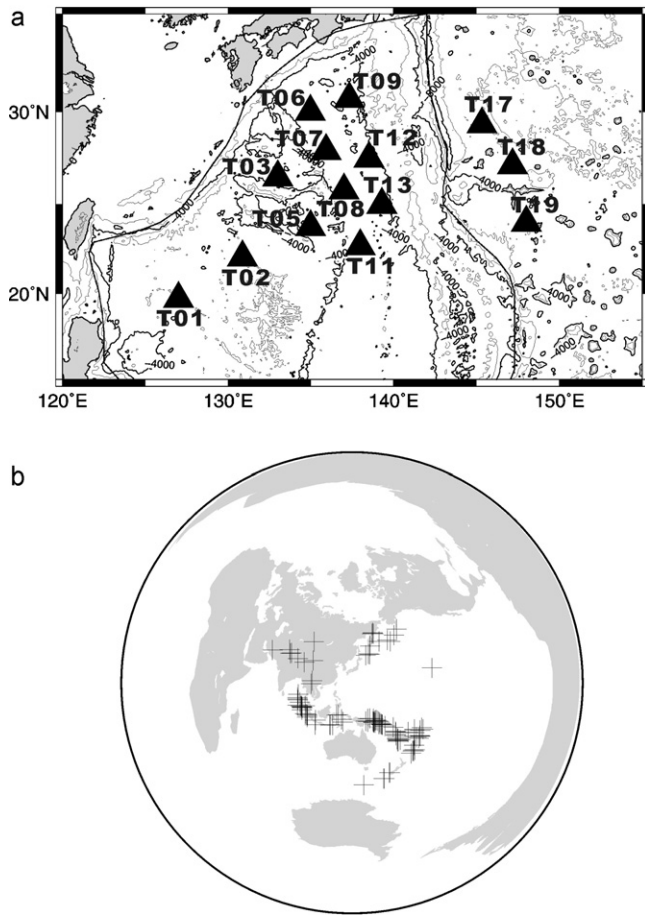E-mail address: dai@jamstec.go.jp (D. Suetsugu).

Figure 1. Station locations (a) and event distribution (b) used in the present study.

Table 1
Coordinates of stations used in the present study.

Station code	Latitude (°N)	Longitude (°E)	Seafloor depth (m)
T01	19.688	127.018	5276
T02	22.047	130.875	5894
T03	26.491	132.999	5328
T05	23.734	134.995	4866
T06	29.989	134.975	4626
T07	27.901	135.924	5265
T08	25.767	137.005	4896
SWSB1	27.767	137.012	4915
SWSB2	27.767	137.012	4915
T09	30.669	137.322	4266
T11	22.670	137.984	4786
T12	27.498	138.513	4688
T13	24.973	139.297	4793
T17	29.326	145.333	5794
T18	27.142	147.174	5582
T19	23.993	148.009	5772

tion of T08. Development of the BBOBSs was commenced in the 1990s by the Earthquake Research Institute, the University of Tokyo (Kanazawa et al., 2001). Each BBOBS has a three-component CMG-3T broadband sensor (Guralp Systems, Ltd.) that continuously records data sampled with 24-bit and 100-Hz resolutions and stores the recorded data in two 40-GB hard disk drives. The observations reveal good spatial coverage of the P-to-S converted waves at the "410" and "660" in the stagnant slab and its vicinity (Fig. 2). The epicentral distances of the earthquakes used here ranged from 30° to 90° (Fig. 1b), and the magnitudes of these earthquakes were greater than 6. In total, 127 earthquakes were selected for the present study.

3. Method

We employed the receiver function method to determine the depths of the "410" and "660." A discontinuity beneath a station is expected to generate a P-to-S converted wave, which arrives after the P wave and is dominant in the radial component. However, in many cases, the Ps waves from the "410" and "660" are not sufficiently large to be analyzed in individual radial-component records; this is because of the small P-to-S conversion coefficient and waveform complexity, which in turn is due to a source effect.
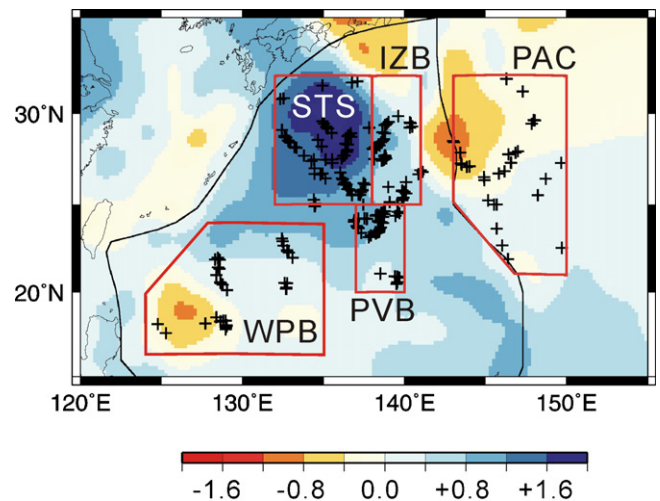
along a subducted slab (Iwamori, 2007; Kawakatsu and Watada, 2007).

In the present study, we address the second possibility described above for the region beneath the Philippine Sea, where the subducted Pacific slab is considered to be horizontal on or below the "660" (stagnant slab) (Okino et al., 1989; Van der Hilst et al., 1991; Fukao et al., 1992, 2001). The stagnant slab covers a large area (500 km × 500 km) in the MTZ, and this facilitates the detection of water in the slab. We employ the methods proposed by Blum and Shen (2004) and Suetsugu et al. (2006) to determine the water content and temperature anomalies in the MTZ; for this determination, we use the seismic velocity as well as depth of the "660." Recent deployment of long-term broadband ocean-bottom seismographs (BBOBSs) in the Philippine Sea enables direct observation of the body waves traveling in the stagnant slab beneath the Philippine Sea.

2. Data

Ocean-bottom geophysical observations were carried out in the Philippine Sea and northwestern Pacific (Shiobara et al., 2009) as part of an interdisciplinary project, "Stagnant Slab Project," which also includes high-pressure experiments and computer simulations (see Section 1 of this special issue). After neglecting the stations where the instruments could not function satisfactorily and/or the data recorded were too noisy, we analyzed the data recorded at 16 BBOBSs for the period 2005–2007, as shown in Fig. 1a and Table 1. Among these BBOBSs, SWSB1 and SWSB2 were in operation before the commencement of the Stagnant Slab Project, and their locations were almost the same as the loca-

Figure 2. Sub-regions. STS (stagnant slab region); IZB (Izu-Bonin Back-arc region); PVB (Parece Vela Basin); WPB (West Philippine Sea basin); PAC (Pacific Ocean). Crosses are P660s piercing points at a depth of 660 km. P-velocity perturbations near "660" (Obayashi et al., 2006) are drawn in the background. The color scale for the P-velocity perturbation is given in percentage.
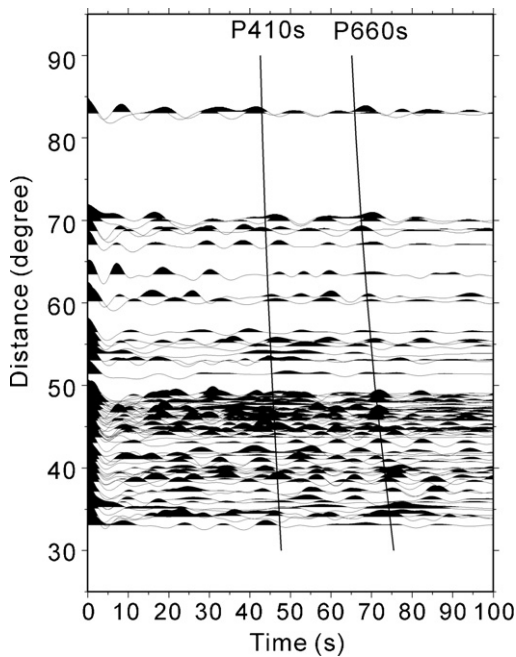
Figure 3. Receiver functions for the stagnant slab region. Theoretical arrival time curves of P410s and P660s computed from the iasp91 model are also shown.

To suppress the source effect, the radial component of a P wave is deconvolved by the vertical-component P wave, which is defined as a receiver function (Langston, 1977; Owens and Crosson, 1988). A low-pass Gaussian filter with a corner period of 10 s is used to reduce the large noise from the oceanic waves. As the source effect is suppressed, we can stack the receiver functions for a number of events having different source processes and thus enhance weak Ps conversion waves. We employ the velocity spectrum stacking (VSS) method (Gurrola et al., 1994) and identify large stacked amplitudes in order to locate discontinuities. The receiver functions for different events are stacked for grids of conversion depths ranging from 0 to 800 km with a 1 km interval and average S velocities ranging from −2.5 to +2.5% with a 0.1% interval; in this interval, we can account for the lateral velocity variations observed beneath the analysis region. The reference model used for the time-to-depth conversion is iasp91 (Kennett and Engdahl, 1991), and the lateral velocity variations are accounted for by using the existing three-dimensional S-velocity models. To compute the average S velocity beneath each station, we use the CRUST2.0 model (Bassin et al., 2000) for the crustal structure and the global S-velocity model (Ritsema and van Heijst, 2000) for the mantle structure. We compute the confidence levels for the discontinuity depths by using the bootstrap method (Efron and Tibshirani, 1986). In this method, the receiver functions are randomly resampled (300 times) prior to stacking. See Suetsugu et al. (2005) for more details.

4. Results

We divided the analysis region into five sub-regions on the basis of tectonic setting, as shown in Fig. 2: the stagnant slab, the Parece Vera Basin (south of the stagnant slab), the West Philippine Sea Basin (southwest of the stagnant slab), the Izu-Bonin Back-arc (east of the stagnant slab), and the northwestern Pacific. We classified the receiver functions into five subsets, which correspond to the aforementioned sub-regions, on the basis of the pierce points of the Ps waves at the "660." Fig. 3 presents the receiver functions for the stagnant slab region. Signal alignments occurred near the expected travel times of the P410s and P660s waves, but their amplitudes

were too small for them to be analyzed individually. We then stacked the receiver functions in each sub-region to enhance the Ps energies from the mantle discontinuities. Fig. 4 shows the stacked amplitudes plotted in the space of the conversion depth and the average S velocity; plus marks denote the "410" and "660" positions identified by assuming average S velocities. Stacked amplitude variation with conversion depth is presented in Fig. 5 to show the statistical significance of the P410s and P660s signals. Fig. 6 shows the estimated depths of the "410" and "660" for the sub-regions. The "410" depth beneath the Pacific Ocean was 396 km, which was shallower than those beneath the Parece Vera basin and the Izu-Bonin back arc regions of the Philippine Sea. This was consistent with the shallow "410" oceanward of the Japan Trench deduced from P-waveform analysis (Obayashi et al., 2006). For the West Philippine Sea Basin and stagnant slab region, the scatter in the receiver functions was large near the "410," and signals from the "410" were below the 95% confidence level. In contrast, signals from the "660" were greater than the confidence level for all sub-regions. The "660" was deepest (691 km) in the stagnant slab region, moderately deep beneath the Parece Vera Basin (674 km) and the West Philippine Sea Basin (670 km) regions, and comparable to the global average (e.g., Flanagan and Shearer, 1998; Gu et al., 2003) beneath the Pacific Ocean (662 km) and the Izu-Bonin Back-arc (659 km). The very deep "660" was confined in the stagnant slab, and there was a sharp contrast in the "660" depths of 20–30 km between the stagnant slab and its surrounding regions. While this contrast has been suggested by previous regional studies that were carried out using triplicated P waves (e.g., Shito and Shibutani, 2001; Tseng and Chen, 2004), the seafloor observation of P660s waves that were directly sampled in the "660" beneath the stagnant slab revealed the abrupt depth change of the "660" in greater detail.

5. Estimation of temperature and water content

We estimate the temperature anomalies and water content in the region immediately above the "660," from the tomographically determined P-velocity anomalies and the "660" depths obtained in the present study. For this purpose, we take into account the equilibrium post-spinel phase change. We assume that the discontinuity depths and P-velocity have a linear dependence on the temperature anomalies and water content. We ignore the effect of anelasticity on the seismic velocity because this effect can be minor in the cool stagnant slab, of which the anelasticity effect is relatively weak. For simplicity, we ignore other compositional factors such as Mg/(Mg+Fe) since the effect of Fe content on the pressure associated with the post-spinel phase change is small (Ito and Takahashi, 1989). We express the velocity perturbation and discontinuity depths in terms of temperature and water content as follows:

$$\delta V = \frac{\partial V}{\partial T}\delta T + \frac{\partial V}{\partial w}\delta w$$
$$\delta d = \frac{\partial d}{\partial T}\delta T + \frac{\partial d}{\partial w}\delta w, \tag{1}$$

where δV and δd are the seismic velocity perturbation (P-velocity perturbation in km/s in the present study) determined from the one-dimensional laterally averaged model of the earth and the deviation of the discontinuity depth from the global average (in km), respectively. We consider 660 km the average "660" depth (Flanagan and Shearer, 1998). The temperature anomaly δT (in K) and water content δw (in wt%) immediately above the "660" are the unknown variables in these equations. The estimated water content and temperature are expressed as relative values with respect to the global average, and therefore, the estimated water content can be a negative value.
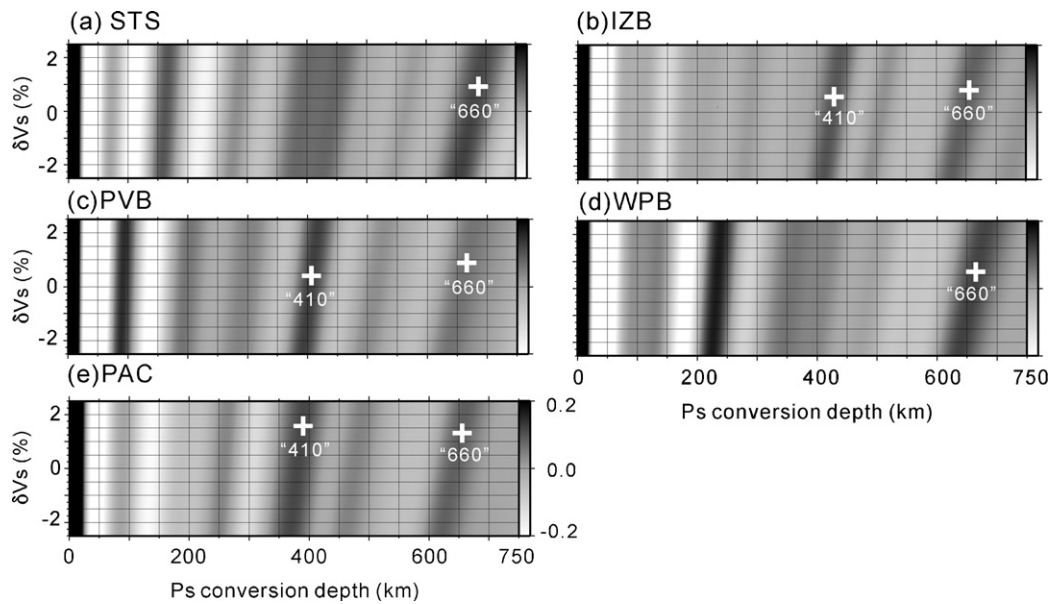
Figure 4. Velocity spectrum stacking (VSS) plots for sub-regions STS, IZB, PVB, WPB, and PAC. The average S-velocity anomalies (vertical axis) are computed using existing S-velocity tomographic models (see text for details). Amplitudes of stacked receiver functions are normalized to 20% of the direct P-wave amplitudes and shown with respect to the Ps conversion depths and average S-wave velocity perturbations. The determined depths of the "410" and "660" are denoted by pluses.
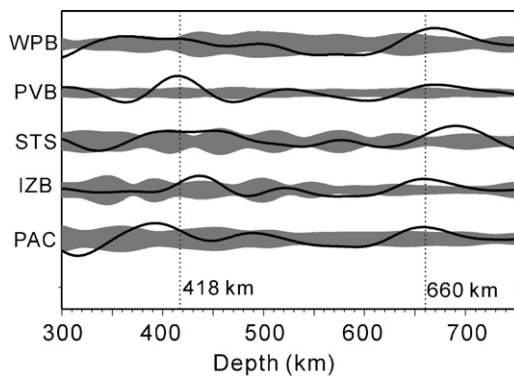

Figure 5. Stacked and depth-converted receiver functions for the sub-regions. The 95% confidence levels are shown by shaded areas.

The partial derivatives $\partial V/\partial T$, $\partial d/\partial T$, $\partial V/\partial w$, and $\partial d/\partial w$ are chosen by referring to experimentally obtained values (Table 2). By assuming the peridotite composition immediately above the "660," we adopt $\partial V/\partial T$ of -3.5×10^{-4} km/s/K in the present study by following Irifune et al. (2008), who reported the temperature dependence of elastic moduli for ringwoodite and majorite (major minerals of the peridotite in the MTZ) under the high pressure and temperature conditions of the MTZ.

The values of $\partial d/\partial T$ are obtained from the Clapeyron slopes of the post-spinel phase change. We tentatively adopt -2.0 MPa/K for the Clapeyron slope in the present study (0.06 km/K for $\partial d/\partial T$). In the discussion, we change the value from -1.0 MPa/K to -3.0 MPa/K to examine the sensitivity of the obtained temperature and water

content to the Clapeyron slope, because experimental values range from about -3 MPa/K (Ito and Takahashi, 1989; Irifune et al., 1998; Akaogi and Ito, 1993) to about -2 MPa/K or smaller (Bina and Helffrich, 1994; Katsura et al., 2003; Fei et al., 2004; Litasov et al., 2005).

We use the partial derivative $\partial d/\partial w$ (dependence of the "660" depth on water content) of 2.7 km/wt% H_2O in the present study. This is based on high-pressure and high-temperature experiments showing that the post-spinel phase boundary is depressed by 8–15 km under water-saturation conditions (e.g., Higo et al., 2001; Litasov et al., 2005). The water content dependence of the discontinuity depths is rather weak, and the estimated temperature and water content are insensitive to the $\partial d/\partial w$ value chosen (Suetsugu et al., 2006) as shown in Section 6.

The partial derivative $\partial V/\partial w$ (which is dependence of P-velocity on water content) may be the most unconstrained parameter of the four partial derivatives in the high pressure and temperature conditions of the MTZ. For ringwoodite, it has been estimated at -0.23 km/s/wt%H_2O from Inoue et al. (1998), -0.15 km/s/wt%H_2O

Table 2
Partial derivatives used in Eq. (1).

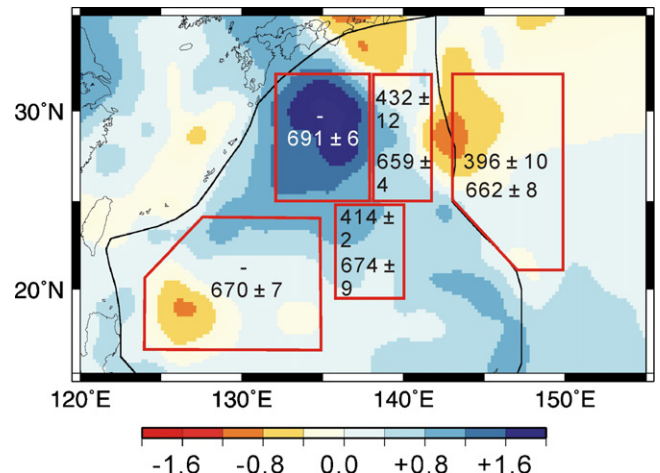|	Dependence on temperature	Dependence on water content
P-velocity	-3.5×10^{-4} km/s/K ($\partial V/\partial T$)	-0.2 km/s/wt% H_2O ($\partial V/\partial w$)
"660" depth	-0.06 km/K ($\partial d/\partial T$)	
Clapeyron slope of -2.0 MPa/K	2.7 km/wt% H_2O ($\partial d/\partial w$)	

Figure 6. "410" and "660" depths for the sub-regions. The color map is same as in Fig. 2.

Table 3
"660" depth, number of data for "660" depth determination, P-velocity anomaly, temperature anomaly, and water content.

Sub-region	"660" depth (km)	Number of data	P-velocity anomaly (km/s)	Temperature anomaly (K)	Water content (wt% H_2O)
Stagnant slab	691 ± 6	76	+0.14 ± 0.02	−508 ± 93	+0.19 ± 0.19
Izu-Bonin Back-arc	659 ± 4	48	+0.03 ± 0.02	+9 ± 62	−0.17 ± 0.14
Parece Vela Basin	674 ± 9	67	+0.06 ± 0.02	−229 ± 139	+0.10 ± 0.26
West Philippine Basin	670 ± 7	41	+0.03 ± 0.02	−161 ± 108	+0.13 ± 0.21
Pacific	662 ± 8	37	0.0 ± 0.02	−31 ± 124	+0.05 ± 0.24

from Wang et al. (2003), and −0.4 km/s/wt% H_2O from Jacobsen et al. (2004) under ambient conditions. Recently, Jacobsen and Smyth (2006) measured sound velocities of ringwoodite at a pressure of 10 GPa (and room temperature) and indicated that hydrous and dry P velocities are similar to each other. The values for majorite, another major component in the MTZ, have not yet been measured. We tentatively adopted −0.2 km/s/wt% H_2O as $\partial V / \partial w$ in the present study, but we will examine the sensitivity of the estimated temperature and water content to $\partial V / \partial w$ in Section 6.

We use the "660" depth deviations from the global average and their standard deviations obtained by the present study (Fig. 6 and Table 3) as δd values and their uncertainties, respectively. The values of δV are taken from the GAP-P1 model (Obayashi et al., 2006). The GAP-P1 model was obtained using more than seven million P first arrival times reported to the Bulletin of the International Seismological Centre (ISC). The model combines the crust and whole mantle of the globe with a block size of $1.4° \times 1.4°$ beneath the western Pacific and Philippine Sea regions. An average velocity perturbation near the "660" is calculated in each sub-region and adopted as δV. The uncertainties in the P velocities are not given in Obayashi et al. (2006). Inoue et al. (1990) estimated the standard deviation of their global P-velocity tomographic model to be 0.05–0.2%, using ISC data similar to those used in Obayashi et al. (2006). In the present study, we adopted a conservative error estimate of 0.2% (0.02 km/s).

Fig. 7 shows the "660" depth deviations obtained in the present study and the P-wave velocity anomalies (Obayashi et al., 2006), along with the isolines of temperature anomalies and water content obtained from Eq. (1) and the partial derivatives. The temperature anomalies vary by 500 K among the five sub-regions, and the water content values are estimated to be around 0.0 wt%, with uncertainties of about 0.2–0.3 wt%. Fig. 8 and Table 3 present the temperature anomalies and water content beneath the sub-regions obtained by solving Eq. (1). Large lateral variations in temperature are observed
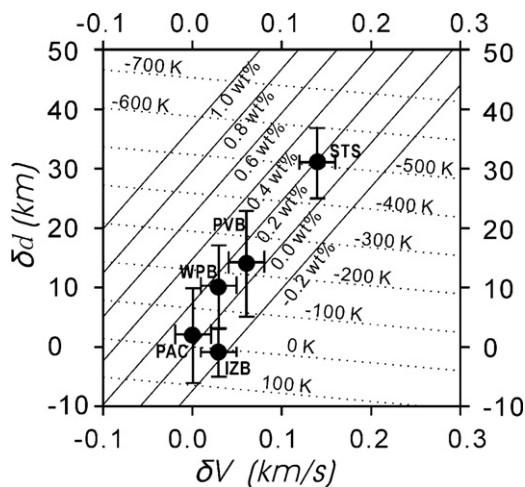
in the analysis region. The temperatures are relatively low in the region beneath the Philippine Sea. The stagnant slab has a temperature anomaly of −500 K, which is the lowest in the studied region. The Parece Vela and west Philippine Sea regions have temperature anomalies of −230 K and −160 K, respectively. The sub-regions near the trench have small temperature anomalies. In contrast, the water content does not differ significantly. It is largest in the stagnant slab (0.19 ± 0.19 wt% H_2O) and smallest in the Izu-Bonin back arc (−0.17 ± 0.14 wt% H_2O). However, the uncertainty levels are ±0.14–0.26 wt% H_2O for the sub-regions and larger than or comparable to the estimates of water content. There is no geographical correlation between the water content and the stagnant slab. While the presence of a small amount of water (less than 0.2 wt% H_2O) is still possible, we did not obtain strong evidence for the transport of water down to the "660" under the Philippine Sea.

6. Discussion

In the present study, we estimate the low-temperature anomalies in the MTZ beneath the Philippine Sea, particularly those in the stagnant slab (500 K). The estimated water content is less than 0.2 wt% H_2O. However, these estimates may be affected by uncertainties in the experimental data used for the partial derivatives and input seismic parameters (the "660" depth and the P-velocity anomaly), as well as those in the linear formulation used in the present study. We discuss in this section how these uncertainties can affect the water content and temperature anomaly.

6.1. Reliability of seismic parameters

This is the first regional study on the topography of the mantle discontinuities beneath the Philippine Sea plate by using BBOBSs. Shito and Shibutani (2001) studied the MTZ structure beneath the Philippine Sea by analyzing complicated P waveforms at land sta-
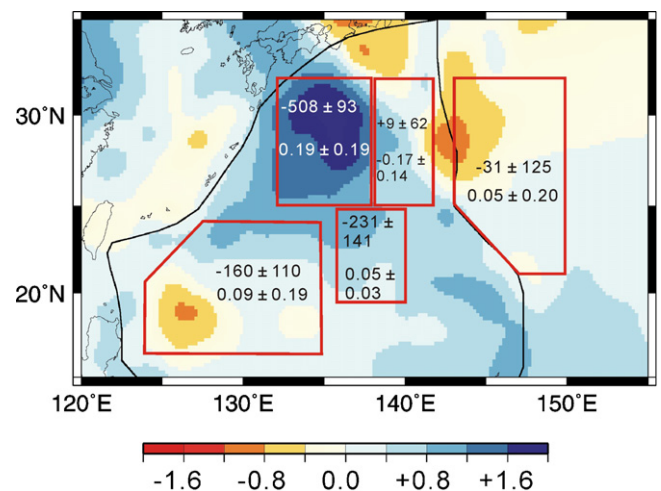

Figure 7. The "660" depth deviations obtained by the present study and the P-wave velocity anomalies (Obayashi et al., 2006) plotted with isolines of temperature anomalies (dotted lines) and water content (solid lines) obtained from Eq. (1) and the partial derivatives.

Figure 8. Temperature anomalies and water content estimated for the sub-regions. In each sub-region, the top number is temperature anomaly and its standard error, and the bottom number is water content and its standard error. The color map is same as in Fig. 2.

tions carried out by triplication of the "410" and "660." Their model AZ41, representing the stagnant slab region, has the "660" at a depth of about 690 km, which is consistent with the "660" depth of 691 ± 6 km for the stagnant slab obtained in the present study. They obtained a normal "660" depth close to the global average in the southern Philippine Sea (south of 20°N), which is consistent with the value acquired in the present study for the West Philippine Sea Basin (670 ± 7 km). In the West Philippine Sea Basin, Suetsugu et al. (2005) obtained 669 ± 9 km for the "660" depth using a receiver function analysis of broadband data recorded at a deep-sea borehole station and a BBOBS station, which is also consistent with the present study. A sharp depth variation of the "660" appears between the stagnant slab region (deep "660") and its southern neighboring regions (normal "660"). Niu et al. (2005) mapped the topography of the "410" and "660" beneath Japan and its vicinity by analyzing land-based Hi-net data of the Japanese islands with the receiver function method. Although their study did not fully cover the stagnant slab beneath the Philippine Sea, they estimated the "660" depth to be 685–690 km and about 660 km beneath the northern end of the stagnant slab region and the northernmost Izu-Bonin Back-arc, respectively. The sharp east-west transition between the stagnant slab and Izu-Bonin Back-arc regions is consistent with that found in the present study. All these results indicate that the deep "660" is confined in the stagnant slab and its depth is about 690 km.

Suetsugu et al. (2006) performed receiver function analysis for the MTZ beneath the Philippine Sea using data from a linear array of long-term semi-broadband ocean-bottom seismographs that were aligned from the Mariana region to the southernmost part of the stagnant slab region from 1999 to 2000. For the Philippine Sea, they obtained "660" depths from 695 km to 708 km along the array and identified a very wet and cold MTZ (1.0–1.4 wt% H_2O, -750 to -550 K) by using the same method as in the present study. Despite the similarity of the studied region, there is a significant difference in the estimated "660" depths and water content between Suetsugu et al. (2006) and the present study. The difference is mainly attributed to different quantities and qualities of seismic data. The sensors used in Suetsugu et al. (2006) had a narrower bandwidth (0.03 s to 30 s) and lower signal-to-noise ratios than those used in the present study, which resulted in much less available data for the receiver function analysis (38 receiver functions in total). We believe that the present estimates of the "660" depths, water content, and temperature anomalies are more reliable than those reported by Suetsugu et al. (2006) for Philippine Sea. Using the "660" depths obtained by previous studies (Niu et al., 2005), Suetsugu et al. (2006) estimated the temperature anomalies and water content in the stagnant slab beneath western Japan to be -300 to -600 K and approximately 0 wt% H_2O, which are consistent with the values obtained in the present study.

The estimated "660" depth can be traded-off with the average S velocity beneath a receiver in VSS that is used for the velocity correction. We used the global S-velocity model by Ritsema and van Heijst (2000) to estimate the average upper mantle S velocities beneath the receivers. When the average velocity in the upper mantle velocity model changes by +1%, the depth of the "660" changes by +8 km and then the estimated temperature and water content change by 120 K and 0.2 wt% H_2O, respectively. Gu et al. (2003) addressed the trade-off problem by performing a joint inversion of $S_{660}S$ and $S_{410}S$ waves with travel times of various body waves and surface waves for long-wavelength mantle S-velocity model and the topographies on the "410" and "660." Comparing results from separate inversions with which the S-velocity and topography were determined independently, they indicated that the S-velocities were not significantly changed by the joint inversion (less than 1%), indicating that the effect of trade-off on the S-velocity is small. We consider that the "660" depth obtained in the

present study is reasonably accurate, and the systematic errors in the temperatures and water content (by errors in the "660" depth) should be less than the abovementioned values (120 K and 0.2 wt% H_2O, respectively).

P-velocity anomalies, the other seismic parameter used for estimating temperatures and water content, could be underestimated by regularization (damping and smoothing) in seismic tomography. To examine whether the tomographic image of the stagnant slab is well reconstructed in the GAP-P1 model, Sugioka et al. (2010) measured the arrival times of P and S waves traveling through the stagnant slab beneath the Philippine Sea using Chinese broadband data from Izu-Bonin deep earthquakes, which are sensitive to the velocity anomalies of the stagnant slab. Theoretical travel time residuals were calculated by accounting for ray bending caused by the three-dimensional velocity variation. The observed negative residuals of P waves are consistent with the theoretical residuals, suggesting that the fast anomalies of the stagnant slab in the GAP-P1 model are reasonably well imaged. The stagnant slab region of the GAP-P1 model has a fast velocity anomaly of $1.4 \pm 0.2\%$ on an average, with a maximum perturbation of 2.1%. This result is consistent with fast anomalies inferred in previous waveform modeling studies (2.0%, Brudzinski and Chen, 1997; 3.0%, Shito and Shibutani, 2001; $1.5 \pm 0.5\%$, Tseng and Chen, 2004).

Another potential source of the systematic error in the P-velocity anomaly is the trade-off with the topography on the "660" depth. In the GAP-P1 model, the topography on the "660" depth is not assumed. The trade-off can be accounted for by jointly inverting P and S wave travel times and Ps-P, however no such study has been performed. Zhao (2004) inverted P-wave travel times for whole mantle three-dimensional velocity model, whose tomographic technique and data are similar to those of the GAP-P1 model. He assumed topography of the Moho, "410," and "660" discontinuities taken from those of the existing models (Mooney et al., 1998; Flanagan and Shearer, 1998), indicating that the trade-off with the topographies results in difference of P-wave velocities by only 0.2%. For the stagnant slab beneath the Philippine Sea, Sugioka et al. (2010) analyzed P-waves, including waves that are propagated through the MTZ sub-horizontally with no interfere with the "660," and showed that the GAP-P1 model provides a good fit to the travel time data as mentioned above. This indicates that the P-velocity anomalies in the MTZ beneath the Philippine Sea are resolved well with little trade-off with the "660" topography. We estimate the systematic error in the P-velocity anomalies to be $\pm 0.2\%$, which could result in ± 0.1 wt% H_2O for water content and ± 4 K for temperatures, which does not change our conclusion.

6.2. Uncertainty in the temperature anomalies and water content

The partial derivatives in Eq. (1) were obtained by experimental studies, and some derivatives are not well constrained. In particular, controversy remains regarding the dependence of the "660" depth on the temperature $\partial d/\partial T$, which is equivalent to the Clapeyron slope of the post-spinel phase transformation, and the dependence of P-velocity on the water content $\partial V/\partial w$. The estimated Clapeyron slope ranges from about -3 MPa/K (Ito and Takahashi, 1989; Akaogi and Ito, 1993; Irifune et al., 1998) to -0.5 MPa/K (Katsura et al., 2003; Fei et al., 2004). The partial derivative $\partial V/\partial w$ has never been obtained in the high pressure and temperature conditions of the MTZ. The value obtained under ambient conditions ranges from -0.15 to -0.4 km/s/wt% H_2O (Inoue et al., 1998; Wang et al., 2003; Jacobsen et al., 2004). Fig. 9 shows the sensitivity of temperature and water content to the partial derivatives in eq. (1). We used the "660" depth and P-velocity anomaly obtained for the stagnant slab region (691 ± 6 km and $1.4 \pm 0.2\%$, respectively) in Fig. 9, while the trend described below can apply to other regions.
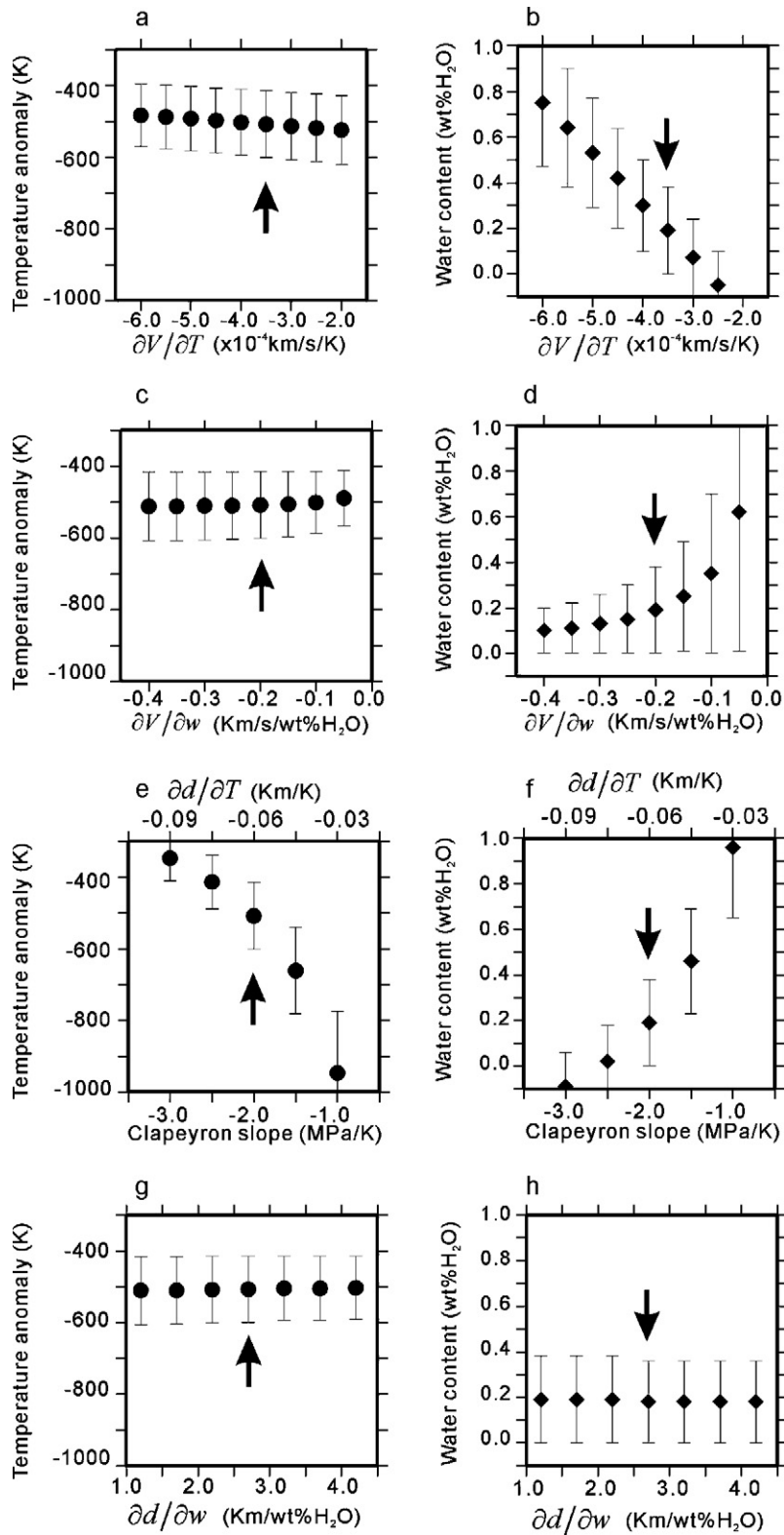
Figure 9. Sensitivity of temperature anomalies and water content to the partial derivatives in Eq. (1). Left four panels show sensitivity to temperature anomalies, and right four show sensitivity to water content. Sensitivities of $\partial V/\partial T$ (a, b); $\partial V/\partial w$ (c, d); $\partial d/\partial T$ (e, f); $\partial d/\partial w$ (g, h) are plotted. Arrows indicate the values of the partial derivatives used in the present study (Table 2).

Temperature estimates are sensitive to the Clapeyron slope (Fig. 9e). Larger absolute values of the slope result from smaller absolute values of the temperature anomaly, and vice versa. This trend is because the temperature anomaly is controlled mostly by the "660" depth in Eq. (1). A Clapeyron slope from −0.5

to −1.0 MPa/K gives a very large negative temperature anomaly (greater than 1000 K) at the "660" in the stagnant slab, which is too large compared with previous estimates of −300 to −600 K, made from observational and simulation studies (e.g., Fukao et al., 2009; Tagawa et al., 2007). Temperature anomalies are not much

affected by the other coefficients (Figs. 9a, c, and g). Estimates of the water content are substantially influenced by changes in $\partial V/\partial T$, $\partial V/\partial w$, and $\partial d/\partial T$ (Figs. 9b, d, and f, respectively). The water content increases for smaller absolute values of the Clapeyron slope (equivalent to $\partial d/\partial T$) and greater absolute values of $\partial V/\partial T$. In particular, a smaller absolute value of $\partial V/\partial w$ gives a greater amount of water, although the associated error also becomes larger (Fig. 9d). Recently Jacobsen and Smyth (2006) showed that P velocities of hydrous and dry ringwoodite are similar, but S velocities are reduced by 2.7% (0.15 km/s) for 1.0 wt% H_2O at the high pressure typical of the MTZ and room temperature. If their result is applicable under the high-temperature conditions of the MTZ, the S velocity could be more useful than the P velocity. In the stagnant slab region, Sugioka et al. (2010) estimated the S-velocity anomalies to be 2.0%. Using $\partial V/\partial T$ of -3.0×10^{-4} km/s/K (Irifune et al., 2008) and $\partial V/\partial w$ of -0.15 km/s/wt% H_2O (Jacobsen and Smyth, 2006) for the S velocity in Eq. (1), the estimated temperature anomaly and water content are -504 ± 92 K and 0.27 ± 0.22 wt% H_2O, respectively, which are comparable to the estimates from the P velocity. The coefficient $\partial d/\partial w$ has little effect on the estimates of temperature or water content.

We have assumed a peridotite composition in the MTZ and ignored the compositional effect on the P-velocity in the present study for simplicity, while it may not be appropriate in a subducted slab (former oceanic lithosphere), which should have a compositional layering from top to bottom, 6–7-km-thick MORB crust, 30–40-km-thick residual harzburgite, and 40–50-km-thick peridotite (e.g., Ringwood and Irifune, 1988), which is formed by partial melting of mantle peridotite at a mid-oceanic ridge (e.g., Green et al., 1979; Ringwood, 1982). Recent sound velocity measurements performed on the slab materials have revealed that the P-velocities in the MORB crust and the residual harzburgite are slightly lower and higher than those in peridotite in the MTZ, respectively (Kono et al., 2007; Nishiyama et al., 2009). However, in the present study, we focus on the stagnant slab immediately above the "660." This is the lower peridotite part of the slab, which should have similar major-element composition to the ambient mantle. We thus reasonably assume that effects of spatial variation in a major-element composition are small in the target depths (650–700 km) of the present study.

6.3. Nonlinearity

We assume a linear relationship in Eq. (1), although some of the partial derivatives may depend on water content. Litasov et al. (2005) estimated the Clapeyron slope of the post-spinel phase change (equivalent to $\partial d/\partial T$) to be in the range -0.5 to -0.8 MPa/K for dry ringwoodite and -2.0 MPa/K for wet ringwoodite. The partial derivatives $\partial V/\partial T$ and $\partial V/\partial w$ could also depend on water content via anelasticity. Water enhances the anelasticity of the minerals in the upper mantle (e.g., Jackson et al., 1992; Karato, 1995), which should reduce seismic velocities through physical dispersion (Kanamori and Anderson, 1977) and increase the dependence of seismic velocities on temperature $\partial V/\partial T$ and water content $\partial V/\partial w$ (e.g., Karato, 1993, 2004; Shito and Shibutani, 2003). Rigorously speaking, the problem needs to be solved by nonlinear techniques [unlike Eq. (1)] using the anelastic (Q) structure in the MTZ beneath the Philippine Sea, which are currently not available. Instead, Suetsugu et al. (2006) has estimated the influence of anelasticity on temperature and water content with Eq. (1) by correcting $\partial V/\partial T$ and $\partial V/\partial w$ for anelasticity with the Q values of PREM (Dziewonski and Anderson, 1981). The anelastic effect does not change the estimate of temperature and water content significantly (+10 K and +0.2 wt% H_2O, respectively). The above estimate of the anelastic effect is, however, highly sensitive to experimental data on the anelasticity of ringwoodite and majorite, though

most of the data is lacking. It is desirable to obtain more experimental data on elasticity and anelasticity and use a fully nonlinear treatment to solve for the temperature and water content.

Recently a non-equilibrium (kinetic) effect on post-spinel phase changes was studied through laboratory experiments under MTZ conditions (e.g., Wang et al., 1997; Kubo et al., 2002). In subducted cold slabs, the phase change is delayed because of slow reaction rates, which could be a partial cause of the deepened "660" in the slab. This kinetic effect on mineralogical phase changes depends strongly on water content (e.g., Kubo et al., 1998) as well as temperature. It is pronounced in dry conditions and reduced by a small amount of water. Kubo et al. (1998) indicated that 0.05 wt% H_2O of water accelerates the phase change substantially. If the kinetic effect is seismologically detected, then it can also be used to estimate the temperature and water content, although this is beyond the scope of the present study.

In the present study we constrained the water content near the "660" beneath the Philippine Sea region by less than 0.2 wt% H_2O, but could not conclude whether the smaller amount of water exists because of large uncertainties in seismic parameters and experimental data. To detect, say, 0.1 wt% H_2O of water with statistical significance, we need to have an accuracy better than ± 3 km for the "660" depths and $\pm 0.2\%$ for the P-velocity anomaly. Though it is not impossible, it is a challenging task when employing the receiver function and tomographic methods. Another method to resolve the small amount of water is to use other geophysical parameters jointly with the seismic parameters. For instance, it could be useful to analyze electrical conductivity in the MTZ simultaneously with the seismic parameters, since dependence of the conductivity on water content, temperature, and major element compositions is different from that of the seismic parameters. It is known that sensitivity to water content may be greater than those of temperature and major element composition under the MTZ condition (e.g., Huang et al., 2005; Dai and Karato, 2009). In a future study, we will analyze the conductivity structure beneath the Philippine Sea together with the seismic structure, because ocean-bottom electromagnetometers were deployed at the same sites as the BBOBS under the Stagnant Slab Project (Shiobara et al., 2009).

7. Conclusions

We determine the "660" depths beneath the Philippine Sea and northwestern Pacific by the receiver function method using the broadband data obtained from BBOBSs. The results are summarized below:

(1) A very deep "660" is present at 691 km, confined to the stagnant slab beneath the Philippine Sea. The surrounding Philippine Sea regions and northwestern Pacific have the "660" at depths of 659–674 km.

(2) Comparison of the "660" depths and P-velocity anomalies indicates that the temperature in the stagnant slab than is lower than that in the MTZ beneath the northwestern Pacific by about 500 K. In the MTZ beneath the Parece Vela Basin and West Philippine Sea Basin, which surround the stagnant slab, the temperature is lower than that beneath the Pacific by about 200 K. The water content beneath the studied area is estimated to be less than 0.2 wt%, which is comparable to or less than the uncertainty in the water content (± 0.2–0.3 wt%). The geographical distribution of the water content is not spatially correlated with the stagnant slab, and there is no clear evidence for the presence of water in the stagnant slab.

(3) More accurate seismological and experimental data are required for a quantitative estimation of small amounts of water (less than the uncertainty level of 0.2 wt% in the present

study) in the MTZ. More in-depth studies must be carried out to determine the dependence of the seismic velocity on the water content under MTZ conditions. Simultaneous analysis of the electrical conductivity of the water present in the MTZ is also expected to be useful to provide tighter constraints to water content, because electrical conductivity is highly sensitive to the water content.

Acknowledgements

References

Akaogi, M., Ito, E., 1993. Refinement of enthalpy measurement of MgSiO$_3$ perovskite and negative pressure–temperature slopes for perovskite-forming reaction. Geophys. Res. Lett. 12, 1839–1842.

Bassin, C., Laske, G., Masters, G., 2000. The current limits of resolution for surface wave tomography in North America. EOS Trans. AGU 81, F897.

Bina, C.R., Helffrich, G., 1994. Phase transition Clapeyron slopes and transition zone seismic discontinuity topography. J. Geophys. Res. 99, 15853–15860.

Blum, J., Shen, Y., 2004. Thermal, hydrous, and mechanical states of the mantle transition zone beneath southern Africa. Earth Planet. Sci. Lett. 217, 367–378.

Bolfan-Casanova, N., Keppler, H., Rubie, D.C., 2003. Water partitioning at 660 km depth and evidence for very low water solubility in magnesium silicate perovskite. Geophys. Res. Lett. 30, doi:10.1029/2003GL017182.

Brudzinski, M.R., Chen, W.-P., 1997. Variations of P wave speeds in the mantle transition zone beneath the northern Philippine Sea. J. Geophys. Res. 102, 11815–11827.

Dixson, J.E., Dixon, T.H., Bell, D.R., Malservisi, R., 2004. Lateral variation in upper mantle viscosity: role of water. Earth Planet. Sci. Lett. 222, 451–467.

Dziewonski, A.M., Anderson, D.L., 1981. Preliminary reference Earth model. Phys. Earth Planet. Inter. 25, 297–356.

Dai, L., Karato, S., 2009. Electrical conductivity of wadsleyite under high pressures and temperatures. Earth Planet. Sci. Lett. 287, 277–283.

Efron, B., Tibshirani, R., 1986. Bootstrap methods for standard errors, confidence intervals, and other measures of statistical accuracy. Stat. Sci. 1, 54–77.

Fei, Y., Orman, J.V., Li, J., van Westrenen, W., Sanloup, C., Minarik, W., Hirose, K., Komabayashi, T., Walter, M., Funakoshi, K., 2004. Experimentally determined postspinel transformation boundary in Mg$_2$SiO$_4$ using MgO as an internal pressure standard and its geophysical implication. J. Geophys. Res. 109, B02305, doi:10.1029/2003JB002562.

Flanagan, M., Shearer, P., 1998. Global mapping of topography on transition zone velocity discontinuities by stacking SS precursors. J. Geophys. Res. 103, 2673–2692.

Fukao, Y., Obayashi, M., Inoue, H., Nenbai, M., 1992. Subducting slabs stagnant in the mantle transition zone. J. Geophys. Res. 97, 4809–4822.

Fukao, Y., Widiyantoro, S., Obayashi, M., 2001. Stagnant slabs in the upper and lower mantle transition zone. Rev. Geophys. 39, 291–323.

Fukao, Y., Obayashi, M., Nakakuki, T., the Deep Slab Project Group, 2009. Stagnant slab: a review. Ann. Rev. Earth Planet. Sci. 37, 19–46.

Green, D.H., Hibberson, W.O., Jaques, A.L., 1979. Petrogenesis of mid-oceanic ridge basalts. In: McElhinny, M.W. (Ed.), The Earth: Its Origin, Structure and Evolution. Academic Press, London, pp. 265–299.

Gu, Y.J., Dziewonski, A.M., Ekström, G., 2003. Simultaneous inversion for mantle shear velocity and topography of transition zone discontinuities. J. Geophys. Res. 154, 559–583.

Gurrola, H., Minster, J.B., Owens, T.J., 1994. The use of velocity spectrum for stacking receiver functions and imaging upper mantle discontinuities. Geophys. J. Int. 117, 427–440.

Higo, Y., Inoue, T., Irifune, T., Yurimoto, H., 2001. Effect of water on the spinel-postspinel transformation in Mg$_2$SiO$_4$. Geophys. Res. Lett. 28, 3505–3508.

Huang, X., Xu, Y., Karato, S., 2005. Water content of the mantle transition zone from the electrical conductivity of wadsleyite and ringwoodite. Nature 434, 746–749.

Ichiki, M., Uyeshima, M., Utada, H., Zhao, G., 2001. Upper mantle conductivity structure of the back-arc region beneath northeastern China. Geophys. Res. Lett. 28, 3773–3776.

Ichiki, M., Baba, K., Obayashi, M., Utada, H., 2006. Water content and geotherm in the upper mantle above the stagnant slab: Interpretation of electrical conductivity and seismic P-wave velocity models. Phys. Earth Planet. Inter. 155, 1–15.

Inoue, H., Fukao, Y., Tanabe, K., Ogata, Y., 1990. Whole mantle P-wave travel time tomography. Phys. Earth Planet. Inter. 59, 294–328.

Inoue, T., Yurimoto, H., Kudoh, Y., 1995. Hydrous modified spinel, Mg$_{1.75}$SiH$_{0.5}$O$_4$: a new water reservoir in the mantle transition region. Geophys. Res. Lett. 22, 117–120.

Inoue, T., Weidner, D.J., Northrup, P.A., Parise, J.B., 1998. Elastic properties of hydrous ringwoodite (γ-phase) on Mg$_2$SiO$_4$. Earth Planet. Sci. Lett. 160, 107–113.

Irifune, T., Nishiyama, N., Kuroda, K., Inoue, T., Isshiki, M., Utsumi, W., Funakoshi, K., Urakawa, S., Uchida, T., Katsura, T., Ohtaka, O., 1998. The post spinel phase boundary in Mg$_2$SiO$_4$ determined by in situ X-ray diffraction. Science 279, 1698–1700.

Ito, E., Takahashi, E., 1989. Postspinel transformations in the system Mg$_2$SiO$_4$–Fe$_2$SiO$_4$ and some geophysical implications. J. Geophys. Res. 94, 10637–10646.

Irifune, T., Higo, Y., Inoue, T., Kono, Y., Ohfuji, H., Funakoshi, K., 2008. Sound velocities of majorite garnet and the composition of the mantle transition region. Nature 451, 814–817, doi:10.1038/nature06551.

Iwamori, H., 2007. Transportation of H$_2$O beneath the Japan arcs and its implications for global water circulation. Chem. Geol. 239, 182–198.

Jackson, I., Paterson, M.S., Fitz Gerald, J.D., 1992. Seismic wave dispersion and attenuation in Aheim dunite. Gephys. J. Int. 108, 517–534.

Jacobsen, S.D., Smyth, J.R., Spetzler, H., Holl, C.M., Frost, D.J., 2004. Sound velocity and elastic constants of iron-bearing hydrous ringwoodite. Phys. Earth Planet. Inter., 143–144, 47–56.

Jacobsen, S.D., Smyth, J.R., 2006. Effect of water on the sound velocities of ringwoodite in the transition zone, geophysical monograph series 167, 'Earth's deep water cycle'. AGU, 131–146.

Kanamori, H., Anderson, D.L., 1977. Importance of physical dispersion in surface-wave and free-oscillation problems, review. Rev. Geophys. Space Phys. 15, 105–112.

Karato, S., 1993. Importance of anelasticity in the interpretation of seismic tomography. Geophys. Res. Lett. 20, 1623–1626.

Karato, S., 1995. Effects of water on seismic wave velocities in the upper mantle. Proc. Jpn. Acad. 71, 61–66.

Karato, S., Jung, H., 1998. Partial melting and the origin of the seismic low velocity and high attenuation zone in the upper mantle. Earth Planet. Sci. Lett. 157, 192–207.

Karato, S., 2004. Mapping water content in upper mantle. In: Eiler, M.J. (Ed.), Inside the Subduction Factory, AGU Geophysical Monograph, 138, pp. 135–152.

Kanazawa, T., Mochizuki, M., Shiobara, H., 2001. Broadband seismometer for a long-term observation on the sea floor. In: Proceedings of the OHP/ION Joint Symposium on Long-term Observations in the Oceans: Current Status and Perspectives for the Future, p. S11-06.

Katsura, T., Yamada, H., Shimei, T., Kubo, A., Ono, S., Kanzaki, M., Yoneda, A., Walter, M.J., Ito, E., Urakawa, S., Funakoshi, K., Utsumi, W., 2003. Post-spinel transition in Mg$_2$SiO$_4$ determined by high P–T in situ X-ray diffractometry. Phys. Earth Planet. Inter. 136, 11–24.

Kawakatsu, H., Watada, S., 2007. Seismic evidence for deep-water transportation in the mantle. Science 316, 1468–1471.

Kelbert, A., Schultz, A., Egbert, G., 2009. Global electromagnetic induction constraints on transition-zone water content variations. Nature 460, 1003–1006.

Kennett, B.L.N., Engdahl, E.R., 1991. Traveltimes for global earthquake location and phase identification. Geophys. J. Int. 105, 429–465.

Kohlstedt, D.L., Keppler, H., Rubie, D.C., 1996. Solubility of water in the α, β and γ phases of (Mg, Fe)$_2$SiO$_4$. Contrib. Miner. Petrol. 123, 345–357.

Kono, Y., Higo, Y., Ohfuji, H., Inoue, T., Irifune, T., 2007. Elastic wave velocities of garnetite with a MORB composition up to 14 GPa. Geophys. Res. Lett. 34, L14308.

Kubo, T., Ohtani, E., Kato, T., Urakawa, S., Suzuki, A., Kanbe, Y., Funakoshi, K., Utsumi, W., Kikegawa, T., Fujino, K., 2002. Mechanisms and kinetics of the postspinel transformation in Mg$_2$SiO$_4$. Phys. Earth Planet. Inter. 129, 153–171.

Kubo, T., Ohtani, E., Kato, T., Shinmei, T., Fujino, K., 1998. Effects of water on the α–β transformation kinetics in San Carlos olivine. Science 281, 85–87.

Langston, C.A., 1977. The effect of planar dipping structure on source and receiver responses for constant ray parameter. Bull. Seismol. Soc. Am. 67, 1029–1050.

Litasov, K.D., Ohtani, E., Sano, A., Suzuki, A., 2005. Wet subduction versus cold subduction. Geophys. Res. Lett. 32, L13312, doi:10.1029/2005GL022921.

Meier, U., Trampert, J., Curtis, A., 2009. Global variations of temperature and water content in the mantle transition zone from higher mode surface waves. Earth Planet. Sci. Lett. 282, 91–101.

Mooney, W.D., Laske, G., Masters, T.G., 1998. CRUST5.1: A global crustal model at $5° \times 5°$. J. Geophys. Res. 103, 727–747.

Mosenfelder, J.L., Deligne, N.I., Asimow, P.D., Rossman, G.R., 2006. Hydrogen incorporation in olivine from 2–12 GPa. Am. Miner. 91, 285–294.

Nishiyama, N., Kato, T., Irifune, T., Wada, K., 2009. Phase relations in harzburgite: stagnation of harzburgite at the lower part of the mantle transition zone and interpretation of seismic discontinuity at 600 km depth. EOS Trans. AGU 90 (52), Fall Meet. Suppl., Abstract DL11A-07.

Niu, F., Levander, A., Ham, S., Obayashi, M., 2005. Mapping the subducting Pacific slab beneath southwest Japan with Hi-net receiver functions. Earth Planet. Sci. Lett. 239, 9–17.

Obayashi, M., Sugioka, H., Yoshimitsu, J., Fukao, Y., 2006. High temperature anomalies oceanward of subducting slabs at the 410-km discontinuity. Earth Planet. Sci. Lett. 243, 149–158.

Ohtani, E., Litasov, K., Hosoya, T., Kubo, T., Kondo, T., 2004. Water transport into deep mantle and formation of a hydrous transition zone. Phys. Earth Planet. Inter., 143–144, 255–269.

Okino, K., Ando, M., Kaneshima, S., Hirahara, K., 1989. The horizontally lying slab. Geophys. Res. Lett. 16, 1059–1062.

Omori, S., Komabayashi, T., Maruyama, S., 2004. Dehydration and earthquakes in the subducting slab: empirical link in intermediate and deep seismic zones. Phys. Earth Planet. Inter. 146, 297–311.

Owens, T.J., Crosson, R.S., 1988. Shallow structure effects on broadband teleseismic P waveforms. Bull. Seismol. Soc. Am. 78, 96–108.

Ringwood, A.E., 1982. Phase transformations and differentiation in subducted lithosphere: Implications for mantle dynamics, basalt petrogenesis, and crustal evolution. J. Geol. 90, 611–643.

Ringwood, A.E., Irifune, T., 1988. Nature of the 650-km seismic discontinuity: implications for mantle dynamics and differentiation. Nature 331, 131–136.

Ritsema, J., van Heijst, H.J., 2000. Seismic imaging of structural heterogeneity in Earth's mantle: evidence for large-scale mantle flow. Sci. Prog. 83, 243–259.

Rüpke, L.H., Phipps Morgan, J., Hort, M., Connolly, J.A.D., 2004. Serpentine and the subduction zone water cycle. Earth Planet. Sci. Lett. 223, 17–34.

Rüpke, L.H., Phipps Morgan, J., Dixon, J.E., 2006. Implications of subduction rehydration for Earth's deep water cycle. In: Jacobsen, S.D., Lee, S.v.d. (Eds.), Earth's Deep Water Cycle. American Geophysical Union, Washington, DC, pp. 263–276.

Shiobara, H., Baba, K., Utada, H., Fuk ao, Y., 2009. Ocean bottom array probes stagnant slab beneath the Philippine Sea. Eos Trans. AGU 90, 70–71.

Shito, A., Shibutani, T., 2001. Upper mantle transition zone structure beneath the Philippine Sea region. Geophys. Res. Lett. 28, 871–874.

Shito, A., Shibutani, T., 2003. Nature of heterogeneity of the upper mantle beneath the northern Philippine Sea as inferred from attenuation and velocity tomography. Phys. Earth Planet. Inter. 140, 331–341.

Shito, A., Karato, S., Matsukage, K.N., Nishihara, Y., 2006. Towards Mapping the three-dimensional distribution of water in the upper mantle from velocity and attenuation tomography, geophysical monograph series 167, 'Earth's deep water cycle'. AGU, 225–236.

Smyth, J.R., 1987. β-Mg_2SiO_4: a potential host for water in the mantle? Am. Miner. 72, 1051–1055.

Suetsugu, D., Shinohara, M., Araki, E., Kanazawa, T., Suyehiro, K., Yamada, T., Nakahigashi, K., Shiobara, H., Sugioka, H., Kawai, K., Fukao, Y., 2005. Determination of mantle discontinuity depths by a receiver function analysis of broadband seismic records from deep-sea borehole observatory and ocean bottom seismograph in the west Philippine Sea basin. Bull. Seism. Soc. Am. 95, 1947–1956.

Suetsugu, D., Inoue, T., Yamada, A., Zhao, D., Obayashi, M., 2006. Towards mapping the three-dimensional distribution of water in the transition zone from P-velocity tomography and 660-km discontinuity depths, geophysical monograph series 167, 'Earth's deep water cycle'. AGU, 237–249.

Sugioka, H., Suetsugu, D., Obayashi, M., Tsuboi, S., Fukao, Y., Gao, Y., 2010. Fast P and S wave velocities associated with the "cold" stagnant slab beneath the northern Philippine Sea. Phys. Earth Planet. Inter. 179, 1–6.

Tagawa, M., Nakakuki, T., Tajima, F., 2007. Dynamical modeling of trench retreat driven by the slab interaction with the mantle transition zone. Earth Planets Space 59, 65–74.

Tatsumi, Y., 1989. Migration of fluid phases and genesis of basalt magmas in subduction zones. J. Geophys. Res. 94, 4697–4707.

Tseng, T.-L., Chen, W.-P., 2004. Contrasts in seismic wave speeds and density across the 660-km discontinuity beneath the Philippine and the Japan Sea. J. Geophys. Res. 109, B04302, doi:10.1029/2003JB002613.

Wang, Y., Martinez, I., Guyot, F., Liebermann, R.C., 1997. The breakdown of olivine to perovskite and magnesiowustite. Science 275, 510–513.

Wang, J., Sinogeikin, S.V., Inoue, T., Bass, J.D., 2003. Elastic properties of hydrous ringwoodite. Am. Miner. 88, 1608–1611.

Wessel, P., Smith, W.H.F., 1998. New, improved version of the generic mapping tool released. EOS Trans. AGU 79, 579.

Williams, Q., Hemley, R.J., 2001. Hydrogen in the deep Earth. Annu. Rev. Earth Planet. Sci. 29, 365–418.

Van der Hilst, R.D., Engdahl, E.R., Spakman, W., Nolet, G., 1991. Tomographic imaging of subducted lithosphere below northwest Pacific island arcs. Nature 353, 37–43.

Van der Meijde, M., Marone, F., Giardini, D., Van der Lee, S., 2003. Seismic evidence for water deep in Earth's upper mantle. Science 300, 1556–1558.

Yamada, A., 2009. Seismological evidence for compositional variations at the base of the mantle transition zone under Japan islands. Godwana Res. 16, 482–490.

Yoshino, T., Manthilake, G., Matsuzaki, T., Katsura, T., 2008. Dry mantle transition zone inferred from the conductivity of wadsleyite and ringwoodite. Nature 451, 326–329.

Zhao, D., 2004. Global tomographic images of mantle plumes and subducting slabs: insight into deep Earth dynamics. Phys. Earth Planet. Inter. 146, 3–34.